

Large-Scale Gravitational Instability and Star Formation in the Large Magellanic Cloud

Chao-Chin Yang, Robert A. Gruendl, and You-Hua Chu

Department of Astronomy, University of Illinois, Urbana, IL 61801

cyang8@astro.uiuc.edu, gruendl@astro.uiuc.edu, chu@astro.uiuc.edu

and

Mordecai-Mark Mac Low

*Department of Astrophysics, American Museum of Natural History, New York,
NY 10024-5192*

mordecai@amnh.org

and

Yasuo Fukui

*Department of Physics and Astrophysics, Nagoya University, Chikusa-ku,
Nagoya 464-8602, Japan*

fukui@a.phys.nagoya-u.ac.jp

ABSTRACT

Large-scale star formation in disk galaxies is hypothesized to be driven by global gravitational instability. The observed gas surface density is commonly used to compute the strength of gravitational instability, but according to this criterion star formation often appears to occur in gravitationally stable regions. One possible reason is that the stellar contribution to the instability has been neglected. We have examined the gravitational instability of the Large Magellanic Cloud (LMC) considering the gas alone, and considering the combination of collisional gas and collisionless stars. We compare the gravitationally unstable regions with the on-going star formation revealed by *Spitzer* observations of young stellar objects. Although only 62% of the massive young stellar object candidates are in regions where the gas alone is unstable, some 85% lie in regions unstable due to the combination of gas and stars. The combined stability

analysis better describes where star formation occurs. In agreement with other observations and numerical models, a small fraction of the star formation occurs in regions with gravitational stability parameter $Q > 1$. We further measure the dependence of the star formation timescale on the strength of gravitational instability, and quantitatively compare it to the exponential dependence expected from numerical simulations.

Subject headings: Galaxies: kinematics and dynamics — galaxies: ISM — galaxies: stellar content — Magellanic Clouds — stars: formation

1. INTRODUCTION

Observations of nearby galaxies suggest that there exists a gas surface density threshold for star formation in a galactic disk (Kennicutt 1989; Martin & Kennicutt 2001). This threshold is hypothesized to be formed by the threshold for gravitational stability of the disk, although alternative explanations have been offered (e.g., Schaye 2004). Gravitationally unstable regions are commonly identified by the Toomre criterion (Toomre 1964; Goldreich & Lynden-Bell 1965), which considers the stability of a single-component disk against axisymmetric perturbations. However, this criterion, when applied to observed gas surface densities, does not always correctly predict the locations of star formation (e.g., Martin & Kennicutt 2001; Wong & Blitz 2002). Stellar contribution to the gravitational instability could be important; for example, the giant molecular clouds in the Large Magellanic Cloud (LMC) have been shown to correlate with stellar surface density, indicating the increase of star formation towards regions of higher stellar gravity (Fukui 2007).

To crudely include the stellar contribution, Jog & Solomon (1984) derived the stability criterion for a two-fluid disk. This stability criterion differs from the Toomre criterion by only a linear correction factor, when the gas-to-stellar ratios of surface density and velocity dispersion are constant across a galaxy, or when the gas and stellar components are only weakly coupled (Wang & Silk 1994). To correctly include the stellar contribution, Gammie (1992) and Rafikov (2001) analyzed the stability of a composite disk consisting of a collisional gas component and a population of collisionless stellar components. The resulting instability criterion has been used to explain the dust morphology of edge-on disk galaxies (Dalcanton, Yoachim, & Bernstein 2004).

We study the relationship between gravitational stability and star formation in the LMC. The LMC is chosen because high linear resolution can be obtained ($1''$ corresponds to 0.25 pc at 50 kpc, Feast 1999), its internal and foreground extinctions are small, and

its moderate inclination allows spatial and kinematical mapping of the disk with minimum confusion along the line of sight. Both stars and the interstellar medium (ISM) of the LMC have been extensively surveyed. Recent *Spitzer Space Telescope* observations have been used to identify massive young stellar objects (YSOs), which mark the sites of current star formation (R. A. Gruendl et al., in preparation; B. A. Whitney et al., in preparation). Massive YSOs provide better probes than H II regions to study the relationship between the ISM and star formation because their stellar energy feedback has not significantly altered the distributions and physical conditions of the ambient ISM.

In this paper, we investigate the relationship between global star formation and gravitational instability in the LMC using two different stability analyses: assuming that the gaseous disk is decoupled from the stellar disk and considering only the gravity of the gas (§ 2.1), or assuming a collisionless stellar disk and a collisional gas disk and using the Rafikov (2001) stability criterion (§ 2.2). The results are discussed in § 3.

2. GRAVITATIONAL INSTABILITY

2.1. Gas Alone

A thin, differentially rotating gaseous disk is unstable against axisymmetric perturbations when

$$Q_g \equiv \frac{\kappa c_g}{\pi G \Sigma_g} < 1, \quad (1)$$

where Q_g is generally referred to as the Toomre Q parameter for a gaseous disk, κ is the epicyclic frequency, c_g is the isothermal sound speed of the gas, G is the gravitational constant, and Σ_g is the unperturbed surface density of the gas (Goldreich & Lynden-Bell 1965).

To apply this analysis to a disk galaxy, approximations need to be made. First, rather than consisting of a single isothermal component, the real ISM consists of gas with temperatures ranging from 10 K to 10^7 K in multiple phases including cold atomic and molecular, warm atomic and ionized, and hot ionized gas. However, the gas mass is dominated by cold atomic and molecular material in turbulent motion, except possibly in star-forming regions where much of the ISM is ionized. Therefore, we consider only the neutral atomic and molecular gas mass. The atomic medium of galaxies generally has nearly constant velocity dispersion (van der Kruit & Shostak 1982; Shostak & van der Kruit 1984; Dickey, Hanson, & Helou 1990; Petric & Rupen 2007), and has a vertical thickness that is well modeled by assuming hydrostatic equilibrium with the gravitational potential at the velocity dispersion (e.g., Malhotra 1995). We assume the gas disk of the LMC has an effective sound speed representative of the velocity dispersion $c_g = 5 \text{ km s}^{-1}$ (Dib, Bell, & Burkert 2006; Petric

& Rupen 2007). Second, Σ_g in equation (1) is the *unperturbed* gas surface density, while the observed gas surface density is *perturbed*. The surface density of a gravitationally unstable region grows exponentially as it collapses; thus, using the observed surface density in equation (1) will correctly diagnose gravitationally unstable regions, but Q_g may be underestimated if collapse has set in. Therefore, we adopt the observed gas surface density for Σ_g in equation (1) to identify gravitationally unstable regions.

The neutral atomic and molecular components of the ISM in the LMC have been well surveyed. For the neutral atomic component, we use the H I column density map derived from the combined data set of the Australia Telescope Compact Array and the Parkes multibeam receiver (Kim et al. 2003). This H I map has a resolution of $\sim 1'$, or 15 pc. For the molecular component, we use the NANTEN CO survey of the LMC conducted by Fukui et al. (1999, 2001). These maps have a resolution of $\sim 2'.6$, or 40 pc. We scale maps of integrated column density by the CO-to-H₂ conversion factor, $X = 5.4 \times 10^{20}$ H₂ atoms cm⁻² (K km s⁻¹)⁻¹ (Blitz et al. 2007) to obtain the H₂ mass distribution. Both the H I and H₂ maps are clipped at the 1σ level to prevent negative densities and minimize the effects of noise. Furthermore, we account for He and heavier elements by assuming that the mass fraction of H is $X \sim 0.7$. From the H I map, we find a total mass for the neutral atomic component of $5.1 \times 10^8 M_\odot$, consistent with the value found by Kim et al. (1998). For the molecular component, we find a total mass of $6.6 \times 10^7 M_\odot$, which is on the high side of the $4\text{--}7 \times 10^7 M_\odot$ given by Mizuno et al. (1999, 2001), as we used a higher CO-to-H₂ conversion factor and included He and heavy elements. We add these two maps to obtain a map of total gas surface density with a resolution of 40 pc pixel⁻¹. The resulting map is shown in Figure 1a.

The remaining parameter needed in equation (1) is the epicyclic frequency κ , defined by

$$\kappa^2 \equiv \frac{2V^2}{R^2} \left(1 + \frac{R}{V} \frac{dV}{dR} \right), \quad (2)$$

where R is the galactocentric distance and $V = V(R)$ is the circular velocity as a function of R . To calculate κ at a given R in the LMC, we use the rotation curve derived by Kim et al. (1998). The rotation curve is a best-fit to the H I and the carbon star (Kunkel et al. 1997) measurements inside and outside of about 3.2 kpc, respectively. We find the derivatives of the circular velocity and thus the epicyclic frequency by central finite differences with an increment of 250 pc, then we use a cubic spline to interpolate the discrete results to a continuous domain. Finally, the center and the orientation of the disk of the LMC need to be specified. To be consistent with the H I kinematics, we adopt the same center and orientation determined by Kim et al. (1998). The kinematic center of the LMC disk is at $\alpha = 05^{\text{h}}17^{\text{m}}6$ and $\delta = -69^\circ 02'$ (J2000) with an inclination of $i = 33^\circ$ and a line of nodes

at a P.A. of -12° . Using this geometry, the total gas surface density map is deprojected to determine the galactocentric distance of each pixel, allowing us to construct a map of Q_g calculated from equation (1). This map is shown in Figure 1b.

The contours in Figure 1b delineate the critical boundary $Q_g = 1$ that surrounds regions gravitationally unstable due to gas alone. Also marked in the figure are candidate massive YSOs from R. A. Gruendl et al. (in preparation), indicating regions of on-going star formation. In the top panel of Figure 2, we show the number distribution of YSO candidates and the corresponding cumulative fraction with respect to Q_g . While $\sim 62\%$ (153 of 245) of the YSO candidates do lie in regions with $Q_g < 1$, the rest are distributed in regions with values as high as $Q_g \sim 3$.

Some of the candidates with $Q_g < 1$ might be argued not to result from large-scale gravitational instabilities because the unstable regions in which they reside are too small. If we exclude regions $\lesssim 100$ pc in diameter, only 47% (116) of the YSO candidates would be associated with gravitationally unstable regions by this criterion. A frequently used empirical correction for the contributions from the stellar component (Jog & Solomon 1984; Wang & Silk 1994) and the effect of the disk scale height (Jog & Solomon 1984) is to raise the critical value to $Q_g \sim 1.4$ (Kennicutt 1989; Martin & Kennicutt 2001). Even if we apply this linear correction factor to the Toomre criterion, $\sim 25\%$ of the YSO candidates still appear to reside in stable regions. Considering the stability of only the gas disk or applying a simple linear correction to the Toomre criterion may not be sufficient to account for star formation activity.

2.2. Gas and Stars Together

We now also consider the contribution of stars to gravitational instability. To include them, we follow Rafikov’s (2001) treatment of a disk galaxy consisting of a collisional gas disk and a collisionless stellar disk. The instability condition becomes

$$\frac{1}{Q_{sg}} \equiv \frac{2}{Q_s} \frac{1}{q} \left[1 - e^{-q^2} I_0(q^2) \right] + \frac{2}{Q_g} R \frac{q}{1 + q^2 R^2} > 1. \quad (3)$$

In equation (3), Q_g is the stability parameter for the gas derived by Goldreich & Lynden-Bell (1965), as defined in equation (1), while

$$Q_s \equiv \frac{\kappa \sigma_s}{\pi G \Sigma_s} \quad (4)$$

is the stability parameter for the stars derived by Toomre (1964), where σ_s is the stellar radial velocity dispersion, Σ_s is the stellar surface density; $R \equiv c_g/\sigma_s$ and $q \equiv k\sigma_s/\kappa$ are two

dimensionless parameters, with k being the wavenumber of the axisymmetric perturbations; and I_0 is the Bessel function of order zero.

Similarly to our procedure in § 2.1, we use local observed values to evaluate Q_{sg} . To estimate the stellar surface density Σ_s , we use the number density of red giant branch (RGB) and asymptotic giant branch (AGB) stars, as they are part of the old stellar population and therefore trace the overall mass distribution of the stellar disk. RGB and AGB stars are luminous and distinctive in the $[J - K_s]$ vs. K_s color-magnitude diagram and much less confused by faint background galaxies or Galactic stars. To select these stars, we follow a procedure similar to that outlined by van der Marel (2001) but use only the Two Micron All Sky Survey Point Source Catalogue (Skrutskie et al. 2006) and the criteria: $[J - K_s] < (22 - [K_s])/10.5$ and $[K_s] < 14.5$. The source counts are then binned with a resolution of 40 pc pixel⁻¹ and Gaussian smoothed with a dispersion of 100 pc. The smoothing scale is chosen to minimize pixel-to-pixel variations due to the small number density of the tracer RGB and AGB stars, while retaining good spatial resolution for the analysis; this scale is also small compared to the large-scale gravitational instability in the analysis. In the resulting map, a faint Galactic background with a gradient is present. Therefore, we fit and subtract this background with exponential and linear dependencies on the Galactic latitude and longitude, respectively. Finally, by adopting the total stellar mass of $2 \times 10^9 M_\odot$ estimated by Kim et al. (1998), we normalize this map to obtain the absolute stellar surface density map shown in Figure 1c (cf. Fig. 2 of van der Marel 2001). We adopt a constant stellar radial velocity dispersion of 15 km s⁻¹, after considering the velocity dispersions of carbon stars (Kunkel et al. 1997; Alves & Nelson 2000; Graff et al. 2000; van der Marel et al. 2002), red supergiants (Prevot et al. 1989; Olsen & Massey 2007), and young globular clusters (Freeman et al. 1983).

With these values assessed, the parameter Q_{sg} defined in equation (3) now depends only on the perturbation wavenumber k , or equivalently, the perturbation wavelength $\lambda = 2\pi/k$ at each pixel (see Fig. 3). Since Q_{sg} decreases with the degree of gravitational instability and our objective is to locate gravitationally unstable regions, we define its value at each pixel as its global minimum with respect to λ . The derived Q_{sg} map of the LMC is shown in Figure 1d, with the identified YSOs overlaid.

Each point is unstable to perturbations over a finite range of wavelengths, as shown by Figure 3. If the size of a gravitationally unstable region is smaller than the minimum unstable wavelength λ_{\min} , no perturbation inside the region can have long enough wavelength to drive an instability. Therefore, we also find λ_{\min} in each pixel, and compare this value with the size of each region containing YSO candidates by visual inspection. The contours of $Q_{sg} = 1$ are plotted over grayscale presentations of λ_{\min} in Figure 4 so that the sizes of

the $Q_{sg} < 1$ regions can be compared with the minimum unstable wavelengths directly.

Figure 1d shows that, because of the stellar contribution, a much larger fraction of the galaxy is unstable than would have been deduced just from the gas contribution shown in Figure 1b. The vast majority of the massive YSO candidates are in fact located within gravitationally unstable regions, in sharp contrast to the results in § 2.1 where only the gas is considered. Particularly noticeable is the vicinity of the LMC bar region, where on-going star formation is observed. This bar region, having low gas surface densities and high epicyclic frequencies, is stable when only the gas disk is considered, but becomes unstable when the stellar component is added. The bottom panel of Figure 2 shows the number distribution of YSO candidates and the corresponding cumulative fraction with respect to Q_{sg} . About 86% (212 of 245) of the YSO candidates are located in regions where $Q_{sg} < 1$. Figure 4 shows 12 of the 212 YSOs in probably stable regions having $Q_{sg} < 1$ but region size $< \lambda_{\min}$. Removing these 12 still leaves 82% of the YSOs whose formation is attributed to gravitational instability of the disk of stars and gas. One caution is that finite thickness of the disk may lower the critical Q_{sg} value slightly, depending on the scale height of the disk relative to the unstable wavelengths (Jog & Solomon 1984). Given an estimated scale height of ~ 180 pc (Kim et al. 1999) and kiloparsec-scale unstable wavelengths in the LMC, this effect may be small. The results demonstrate that the stellar contribution to gravitational instability can be significant. Gravitational instability of the full disk appears responsible for most large-scale star formation activity.

3. DISCUSSION AND CONCLUSIONS

Schaye (2004) has argued that a constant gas surface density threshold is a good indicator in predicting the edge of the star forming disk. He suggested that, for the LMC disk, this threshold is $\sim 4 M_{\odot} \text{ pc}^{-2}$. Figure 1a shows the contours of $4 M_{\odot} \text{ pc}^{-2}$ in total neutral gas surface density. The contours encompass the majority of the LMC disk except the central cavities of the supergiant shells LMC-4 and LMC-8 (Meaburn 1980). Clearly, all the massive YSO candidates are located where the gas surface density is greater than $4 M_{\odot} \text{ pc}^{-2}$, but this constant surface density threshold does not account for the distribution of the star forming sites, especially in the inner parts of the LMC disk. Therefore, Schaye’s (2004) constant surface density threshold is a necessary but not sufficient condition for star formation. Detailed analysis of the large-scale gravitational instability, as shown in § 2, is still needed.

Another measure of the response of star formation to disk instability is the relation between Q_{sg} and the effective timescale for star formation τ_{sf} . This can be approximated if

we assume the average lifetime of massive YSOs is constant. We normalize the number of YSOs, N_* , within a region having a given range of Q_{sg} by the area, as represented by the total number of pixels N_{pix} within that region. Figure 5 presents N_*/N_{pix} , which is $\propto \tau_{sf}^{-1}$, for a number of Q_{sg} bins. The errors in the ratio are estimated assuming Poisson statistics on the number of YSOs and number of pixels, while the horizontal error bars show the size of the bins. A clear log-linear relationship is found, implying that the response of star formation depends exponentially on the value of Q_{sg} . Li, Mac Low, & Klessen (2005) also found an exponential dependence $\tau_{sf} \propto \exp(\alpha Q_{sg})$, with $\alpha = 4.2 \pm 0.3$ from global numerical simulations of galactic disks. A linear fit to the data in Figure 5 gives a slope that can be interpreted as a local value of $\alpha = 2.7 \pm 0.2$. This behavior appears to be a general property of nonlinear gravitational instability.

We have made the simple assumption that the structure of the LMC is a thin, flat disk with negligible stellar halo. In reality, tidal features due to galaxy-galaxy interactions do exist in the outer parts of the disk (e.g., van der Marel 2001). Furthermore, at some locations, there exist multiple H I velocity components, which we have simply summed to obtain total gas surface density. Other uncertainties stem from our assumed constant gas effective sound speed (or velocity dispersion) and stellar radial velocity dispersion. These affect the relative contribution of each component to the gravitational instability: the higher the local velocity dispersion, the less contribution a component has. The sound speed of the gas we adopt, 5 km s^{-1} , is a typical average for the neutral gas. The radial velocity dispersion of stars is also uncertain. As gravitational instability is much more sensitive to the gas component due to its low sound speed, it is less affected by the uncertainty in the stellar velocity dispersion. Yet another effect to consider is the scale height of the disk, which tends to stabilize the disk (Toomre 1964; Jog & Solomon 1984). Given all these uncertainties, nevertheless, the exponential dependence of star formation rate on Q_{sg} that we find appears to be robust.

From our analysis of the gravitational instability of the LMC, we conclude that the contribution of the stellar disk to gravitational instability cannot be ignored (Jog & Solomon 1984; Gammie 1992; Rafikov 2001). Taking it into account in the case of the LMC, we find that $\sim 85\%$ of the massive YSO candidates lie in gravitationally unstable regions, implying that star formation occurs predominantly in these regions. It appears that gravitational instability of the disk drives most large-scale star formation, as proposed by Elmegreen (2002), Kravtsov (2003), and Li et al. (2005).

This research was supported by NASA grants JPL1264494 and JPL1290956, and NSF grant AST03-07854. We would like to thank Dr. Charles Gammie for his feedback and discussions in this work. We also thank the anonymous referee for the prompt review and useful suggestions.

REFERENCES

- Alves, D. R., & Nelson, C. A. 2000, *ApJ*, 542, 789
- Blitz, L., Fukui, Y., Kawamura, A., Leroy, A., Mizuno, N., & Rosolowsky, E. 2007, in *Protostars and Planets V*, ed. B. Reipurth, D. Jewitt, & K. Keil (Tucson: Univ. of Arizona Press), 81 (astro-ph/0602600)
- Dalcanton, J. J., Yoachim, P., & Bernstein, R. A. 2004, *ApJ*, 608, 189
- Dib, S., Bell, E., & Burkert, A. 2006, *ApJ*, 638, 797
- Dickey, J. M., Hanson, M. M., & Helou, G. 1990, *ApJ*, 352, 522
- Elmegreen, B. G. 2002, *ApJ*, 577, 206
- Feast, M. 1999, in *IAU Symp. 190, New Views of the Magellanic Clouds*, ed. Y.-H. Chu, N. B. Suntzeff, J. E. Hesser & D. A. Bohlender (San Francisco: ASP), 542
- Freeman, K. C., Illingworth, G., & Oemler, A., Jr. 1983, *ApJ*, 272, 488
- Fukui, Y. 2007, in *IAU Symp. 237, Triggered Star Formation in a Turbulent ISM*, ed. B. G. Elmegreen & J. Palous (Cambridge: Cambridge Univ. Press), 31
- Fukui, Y., Mizuno, N., Yamaguchi, R., Mizuno, A., & Onishi, T. 2001, *PASJ*, 53, L41
- Fukui, Y., et al. 1999, *PASJ*, 51, 745
- Gammie, C. F. 1992, Ph.D. Thesis, Princeton University
- Goldreich, P., & Lynden-Bell, D. 1965, *MNRAS*, 130, 97
- Graff, D. S., Gould, A. P., Suntzeff, N. B., Schommer, R. A., & Hardy, E. 2000, *ApJ*, 540, 211
- Jog, C. J., & Solomon, P. M. 1984, *ApJ*, 276, 114
- Kennicutt, R. C., Jr. 1989, *ApJ*, 344, 685
- Kim, S., Staveley-Smith, L., Dopita, M. A., Freeman, K. C., Sault, R. J., Kesteven, M. J., & McConnell, D. 1998, *ApJ*, 503, 674
- Kim, S., Dopita, M. A., Staveley-Smith, L., & Bessell, M. S. 1999, *AJ*, 118, 2797
- Kim, S., Staveley-Smith, L., Dopita, M. A., Sault, R. J., Freeman, K. C., Lee, Y., & Chu, Y.-H. 2003, *ApJS*, 148, 473

- Kravtsov, A. V. 2003, *ApJ*, 590, L1
- Kunkel, W. E., Demers, S., Irwin, M. J., & Albert, L. 1997, *ApJ*, 488, L129
- Li, Y., Mac Low, M.-M., & Klessen, R. S. 2005, *ApJ*, 626, 823
- Malhotra, S. 1995, *ApJ*, 448, 138
- Martin, C. L., & Kennicutt, R. C., Jr. 2001, *ApJ*, 555, 301
- Meaburn, J. 1980, *MNRAS*, 192, 365
- Mizuno, N., et al. 1999, in *Star Formation 1999*, ed. T. Nakamoto (Nobeyama:Nobeyama Radio Observatory), 56
- Mizuno, N., et al. 2001, *PASJ*, 53, 971
- Olsen, K. A. G., & Massey, P. 2007, *ApJ*, 656, L61
- Petric, A. O., & Rupen, M. P. 2007, *AJ*, in press (astro-ph/0704.0279)
- Prevot, L., Martin, N., & Rousseau, J. 1989, *A&A*, 225, 303
- Rafikov, R. R. 2001, *MNRAS*, 323, 445
- Schaye, J. 2004, *ApJ*, 609, 667
- Shostak, G. S., & van der Kruit, P. C. 1984, *A&A*, 132, 20
- Skrutskie, M. F., et al. 2006, *AJ*, 131, 1163
- Toomre, A. 1964, *ApJ*, 139, 1217
- van der Kruit, P. C., & Shostak, G. S. 1982, *A&A*, 105, 351
- van der Marel, R. P. 2001, *AJ*, 122, 1827
- van der Marel, R. P., Alves, D. R., Hardy, E., & Suntzeff, N. B. 2002, *AJ*, 124, 2639
- Wang, B., & Silk, J. 1994, *ApJ*, 427, 759
- Wong, T., & Blitz, L. 2002, *ApJ*, 569, 157

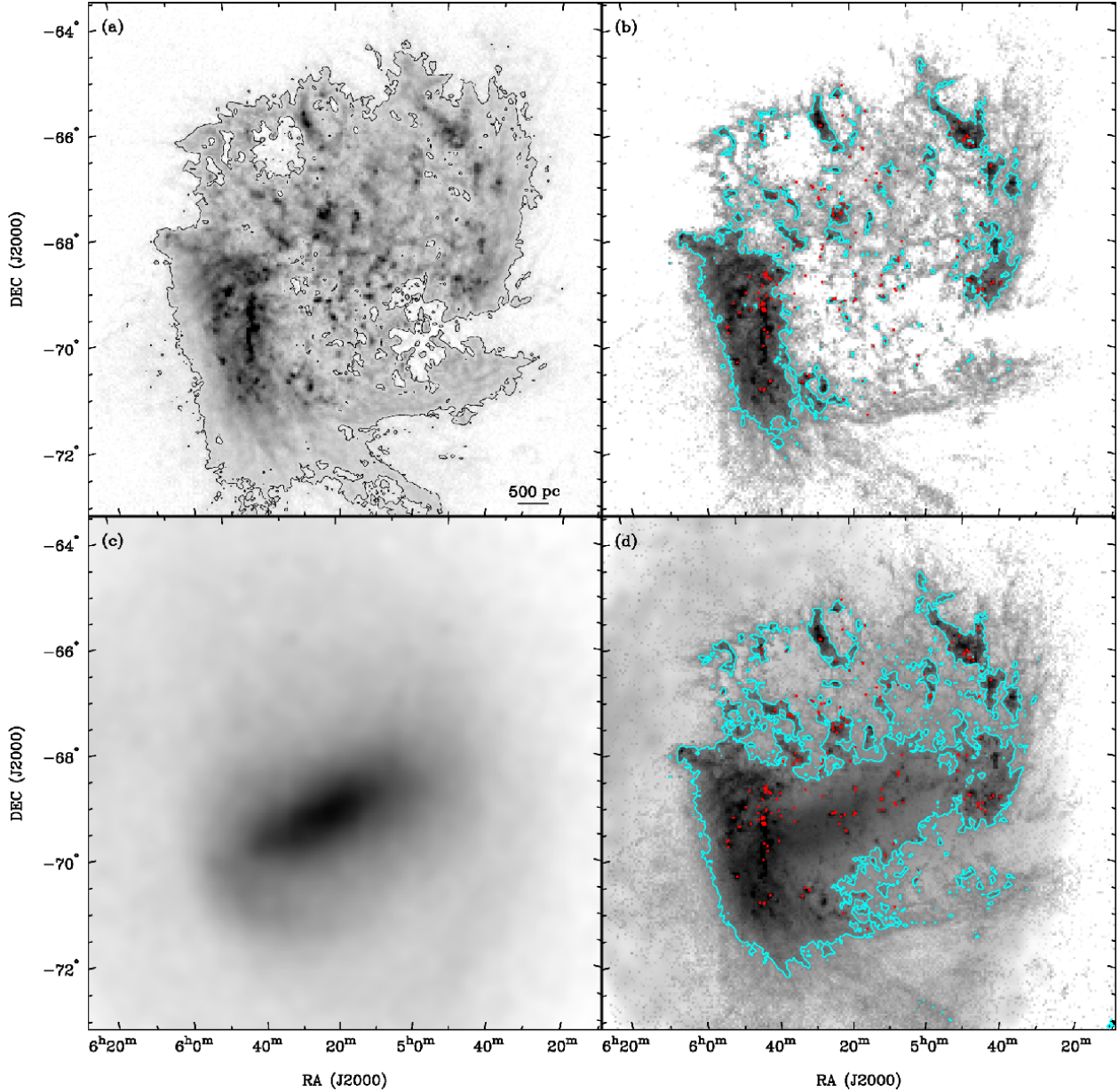


Fig. 1.— (a) Total gas surface density distribution in the Large Magellanic Cloud. Only neutral species are included in this map. The grayscale runs linearly from 0 to $100 M_\odot \text{pc}^{-2}$. The contour lines show a surface density of $4 M_\odot \text{pc}^{-2}$. (b) Comparison between massive star-forming sites traced by young stellar object candidates (*red dots*) and regions where the gas alone is gravitationally unstable. The Toomre parameter for the gas Q_g is shown in grayscale, running logarithmically from 5.0 to 0.2. The *solid* lines delineate the critical value of $Q_g = 1$ inside which the regions are gravitationally unstable. (c) Total stellar surface density distribution. The grayscale runs linearly from 0 to $200 M_\odot \text{pc}^{-2}$. (d) As in (b), but for regions where the gas and stars together are gravitationally unstable, rather than just the gas alone.

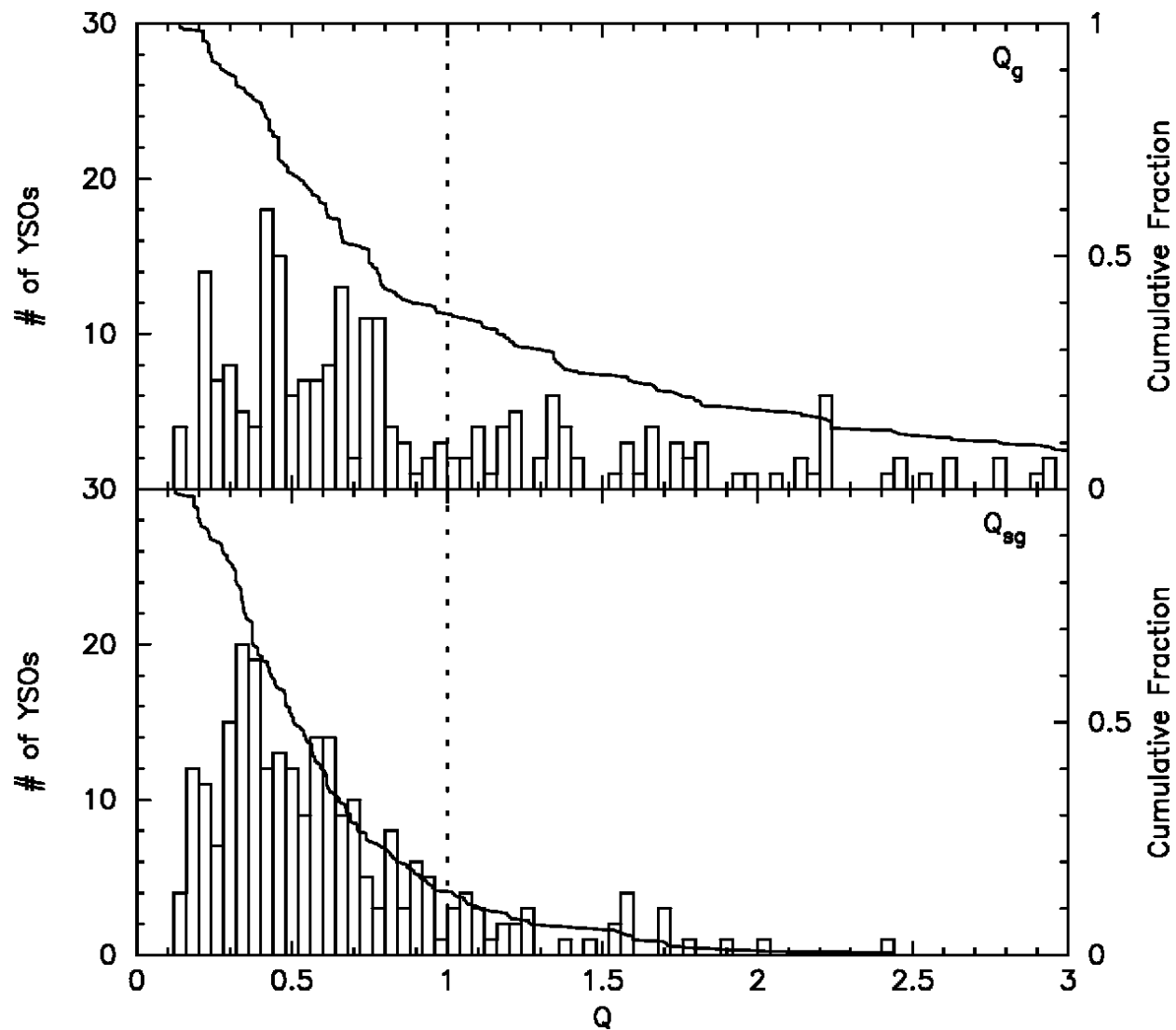


Fig. 2.— Number distribution of YSO candidates with respect to the Toomre stability parameter of the pixel in which they are located. The *top* and *bottom* panels show respectively the Toomre parameters for the gas alone Q_g , and the stars and gas together Q_{sg} . The *solid* lines show the cumulative fractions of YSOs with decreasing Q . The vertical *dotted* lines denote the critical value $Q = 1$.

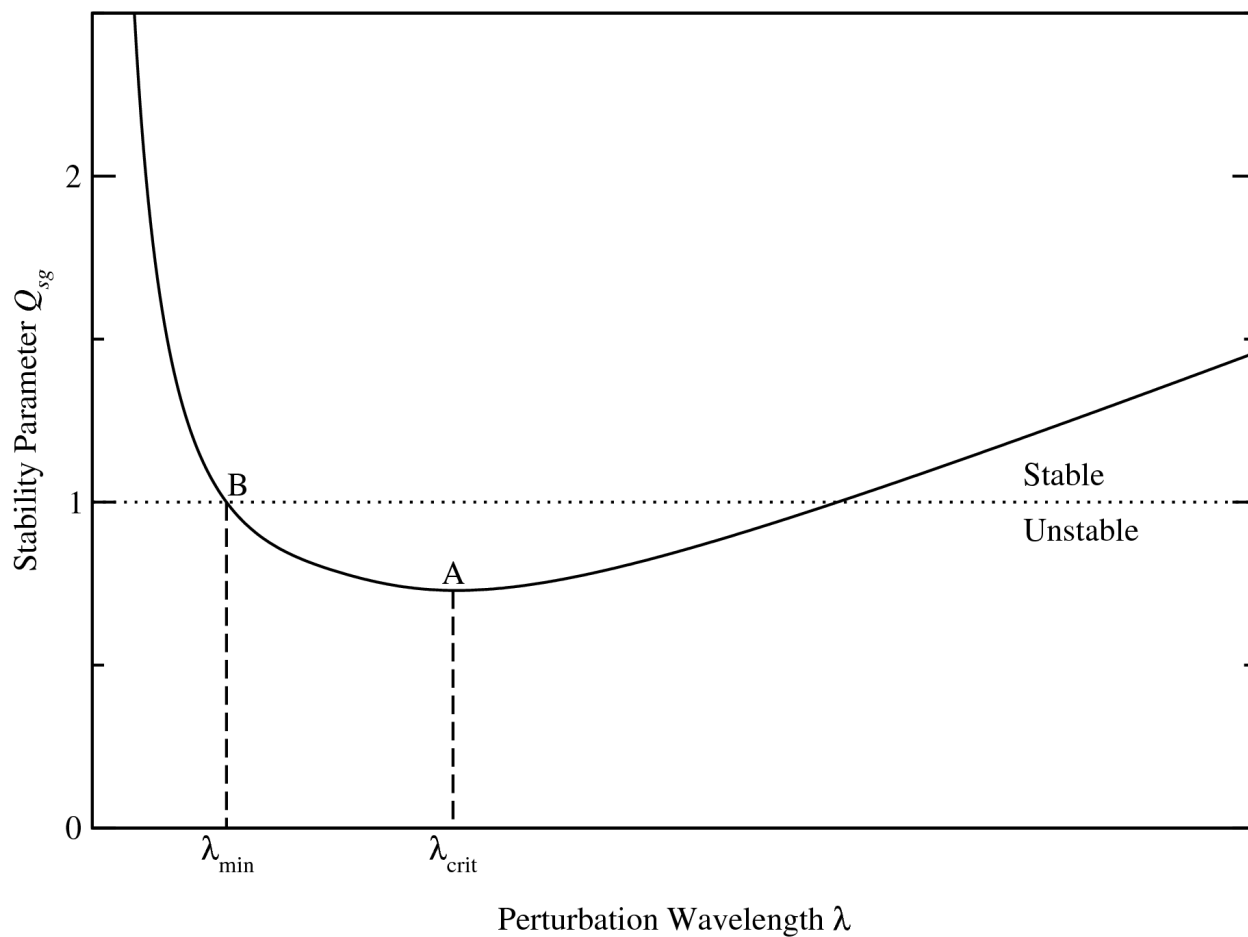


Fig. 3.— Schematic plot of the Q_{sg} parameter as a function of wavelength λ of radial perturbations. The disk of stars and gas is stable against perturbation of a given λ when $Q_{sg} > 1$; otherwise, it is unstable. We measure the value of Q_{sg} at its minimum in each pixel, occurring at $\lambda = \lambda_{\text{crit}}$ (point A). We also find the minimum wavelength λ_{\min} such that the disk is marginally unstable (point B).

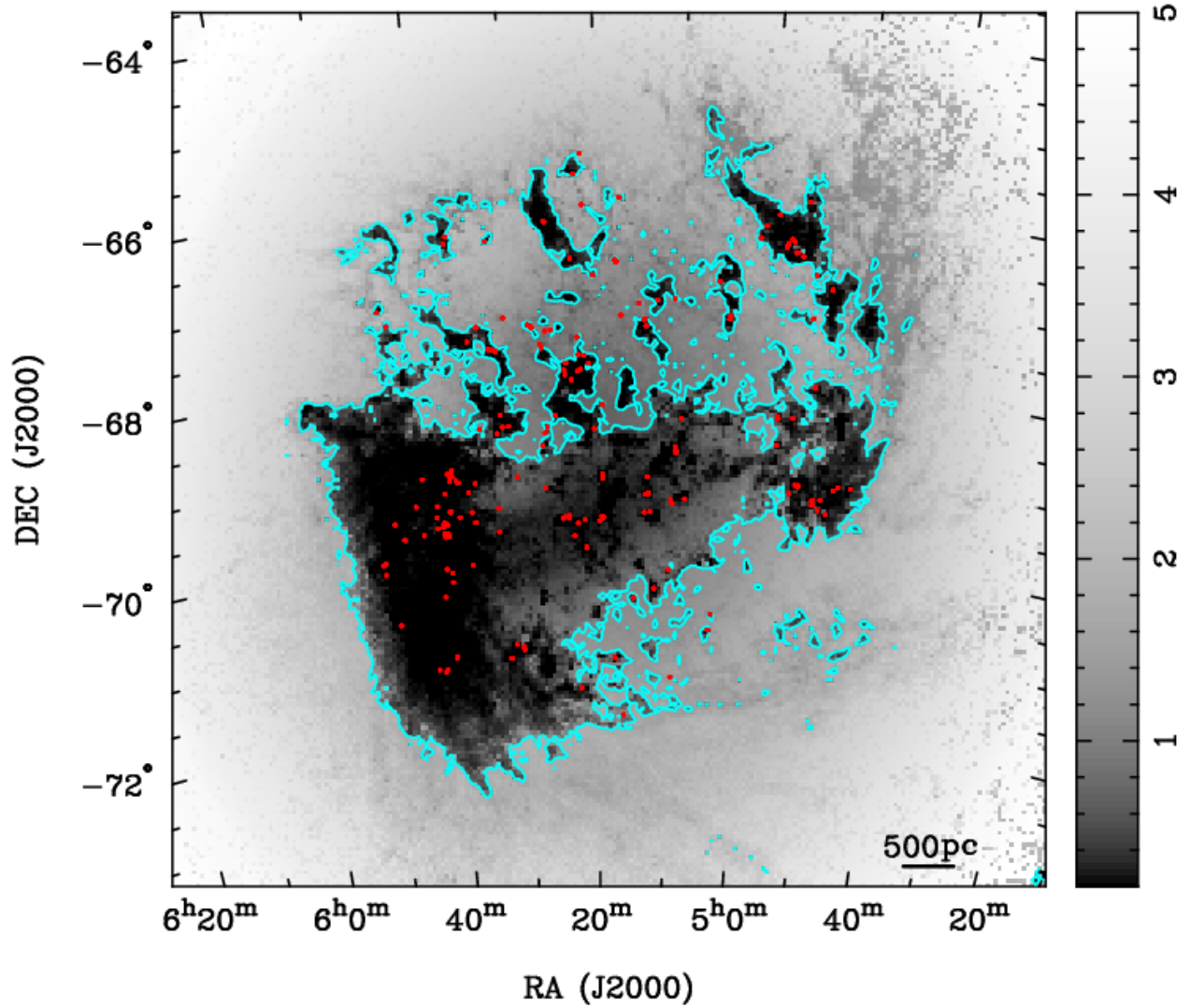


Fig. 4.— Map of the minimum unstable wavelength λ_{\min} , shown in grayscale. The solid contours delineate the critical boundary of $Q_{sg} = 1$, while the red dots mark the massive YSO candidates. λ_{\min} is defined by λ_{crit} (see Fig. 3) when $Q_{sg} > 1$.

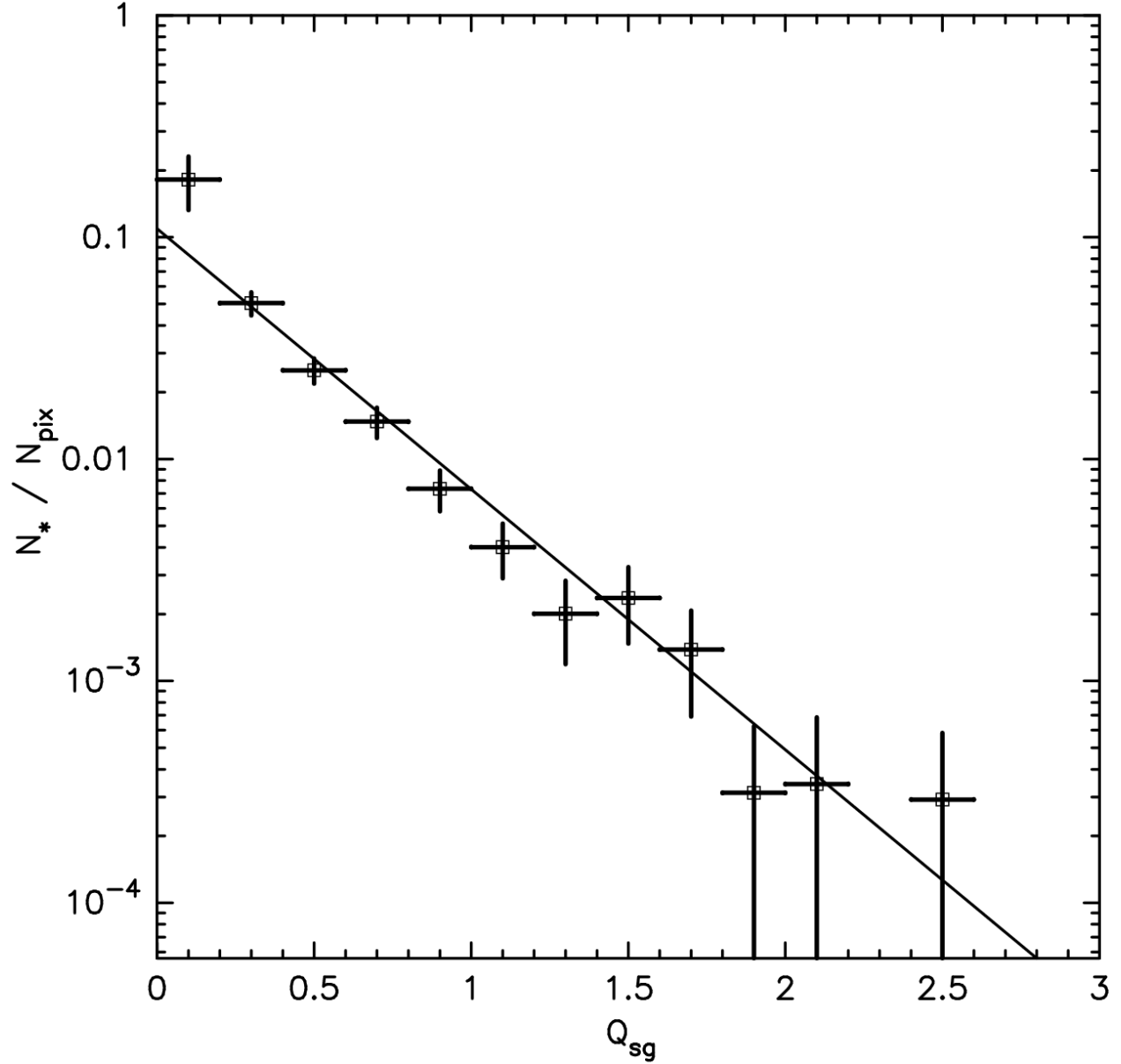


Fig. 5.— Ratio of the number of YSO candidates N_* to the number of pixels N_{pix} in each Q_{sg} bin, denoted by squares. The vertical error bars are estimated by Poisson statistics, while the horizontal error bars show the bin sizes. The *solid* line is the best-fit, of slope -2.7 ± 0.2 .